Nanoscale Res Lett (2007) 2:107–111
DOI 10.1007/s11671-007-9039-7

NANO IDEAS

Fabrication of CuO nanoparticle interlinked microsphere cages by solution method

Jian Quan Qi · Hu Yong Tian · Long Tu Li · Helen Lai Wah Chan

Published online: 3 February 2007

Abstract Here we report a very simple method to convert conventional CuO powders to nanoparticle interlinked microsphere cages by solution method. CuO is dissolved into aqueous ammonia, and the solution is diluted by alcohol and dip coating onto a glass substrate. Drying at 80 °C, the nanostructures with bunchy nanoparticles of $Cu(OH)_2$ can be formed. After the substrate immerges into the solution and we vaporize the solution, hollow microspheres can be formed onto the substrate. There are three phases in the as-prepared samples, monoclinic tenorite CuO, orthorhombic $Cu(OH)_2$, and monoclinic carbonatodiamminecopper(II) ($Cu(NH_3)_2CO_3$). After annealing at 150 °C, the products convert to CuO completely. At annealing temperature above 350 °C, the hollow microspheres became nanoparticle interlinked cages.

Keywords CuO · Microsphere · Narnoparticle

Introduction

Cupric oxide, CuO, has a monoclinic crystal structure. It has many interesting properties and received much research attention [1–18]. CuO is a p-type semiconductor in general with a narrow band gap (1.2 eV) [18, 19] and hence is potentially useful for constructing junction devices such as p-n junction diodes [20]. Recent studies indicate that CuO can exist in three different magnetic phases: a three-dimensional collinear antiferromagnetic phase at temperatures under 213 K, an intermediate noncollinear incommensurate magnetic phase between 213 and 230 K and a one-dimensional quantum antiferromagnetic phase at temperatures above 230 K [11, 21]. CuO-supported catalysts have shown excellent activity for NO_x abatement with different reducing agents, such as CO [22], hydrocarbons [23], or ammonia [7]. Based on its unique properties, CuO, especially with nanostructures has widespread applications, such as high-temperature superconductors [24, 25], optical switch [18], anode electrodes for batteries [4, 26], heterogenous catalysts for several environmental processes [4, 22, 23, 27, 28], solid state gas sensor heterocontacts [29, 30], and microwave dielectric materials [31].

Recently, nanostructured CuO has been studied intensely and different morphologies, such as nanowires, nanoribbons, nanobelts, nanofibers, nanotubes and so on have been synthesized. Among these, chemical vapor deposition (CVD) [32], laser vaporization, electrochemical techniques [33, 34], hydrothermal treatment [35] and the exfoliating method [36] have been documented. In these methods, costly equipment or high temperature is involved and thus decreased the chemical activity of CuO. In this study, we reported a simple and low cost approach to convert conventional CuO to nanoparticle interlinked microsphere cages near room temperature by a solution method. As far as we known, this kind of microsphere cages was not reported previously, and it can have special applications potentially.

J. Q. Qi (✉) · L. T. Li
Department of Materials Sciences and Engineering, Tsinghua University, Beijing 100084, China
e-mail: jianquanqi@mail.tsinghua.edu.cn

J. Q. Qi · H. Y. Tian · H. L. W. Chan
Department of Applied Physics and Materials Research Center, The Hong Kong Polytechnic University, Hong Kong, China

Experimental

Fabrication of CuO nanoparticle interlinked microsphere cages can be very simple by conversion of conventional CuO in solution and similar to that of converting conventional NiO to nanostructures as we have reported previously [37]. Nanostructures of $Cu(OH)_2$ and CuO were converted from conventional CuO powders by a process as follows: 0.5 g copper oxide (BDH Chem. Ltd., UK) was dissolved in 100 ml of 25% aqueous ammonia (International Laboratory, USA). After 24 h of dissolving, the solution turned to a blue colour. The above copper solution was diluted into 500 ml by ethanol absolute, then dip coated on a conventional sodium glass substrate, followed by drying at 80 °C in an oven. In order to obtain enough quantity of CuO on the substrate, the substrate immerged into the solution and then the solution on the substrate was vaporized. Finally, the samples were annealed at different temperatures.

The X-ray diffraction (XRD) patterns of the samples were measured with a Philips X'Pert diffractometer in Bragg–Brentano reflection geometry using CuKα radiation at a scan rate of 0.05 $^0 2\theta$/s. The crystallization behavior of the as-prepared sample was monitored using a differential thermal analysis-thermogravimetric (TG-DTA) instrument (Netzsch STA 449C) with a temperature increase rate of 10 °C/min from room temperature up to 900 °C. Field emission scanning electron microscopy (FE-SEM, JSM 6335F NT) was used to analyze the particle size and morphology of the samples.

Results and discussion

The dissolving of raw CuO powders in ammonia is expessed in Eq. 1. The evaporation process at 80 °C produces $Cu(OH)_2$ and CuO by decomposing the products in Eq. 1.

$$CuO + nNH_3 + H_2O \rightarrow Cu(NH_3)_n^{2+} + 2OH^- \quad (1)$$

Here ''n'' may be equal to 2, 4, 5, 6 but 4 is preferable. The solubility of CuO in aqueous ammonia increases with CO_2 in air because $Cu(NH_3)_2CO_3$ is produced in the solution. Part of the as-prepared powders turned to black after prolonged drying even at as low as 80 °C because $Cu(OH)_2$ decomposed into black CuO. Upon annealing at higher temperatures, both $Cu(OH)_2$ and $Cu(NH_3)_2CO_3$ further decomposed into CuO.

Figure 1 shows a representative FE-SEM image of the as-prepared samples dip coated once. The precipitations are blue and can be identified as $Cu(OH)_2$ by the XRD analysis. It is clearly shown that nanostructures with bunchy nanoparticles of $Cu(OH)_2$ have been formed. The nanoparticles are round and uniform with a size of about 50 nm as shown in Fig 1.

When the solution was vaporized in the air (putting the beaker with the solutions opening for a long time), the precipitations can formed and floated on the surface of the solutions but not precipitated down to the bottom of beakers, we can imagine that the precipitations were taken onto the surface of the solutions by ammonia gas. Figure 2 shows a representative image of the samples which were prepared by vaporizing the solution on the substrate after annealing at 150 °C. It is amazing that microspheres were

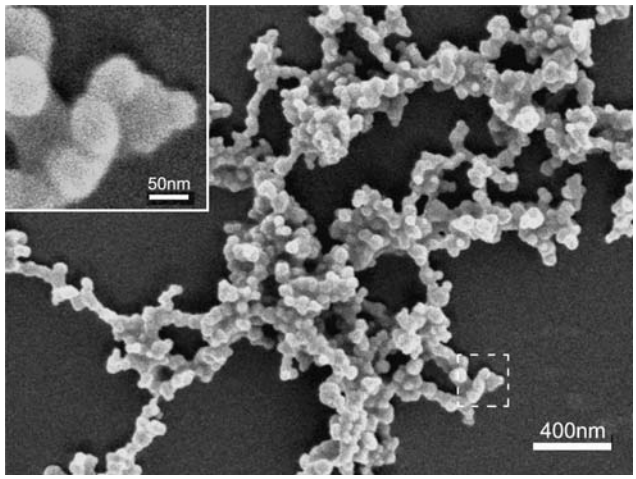

Fig. 1 The samples dip coated once in alcohol solution

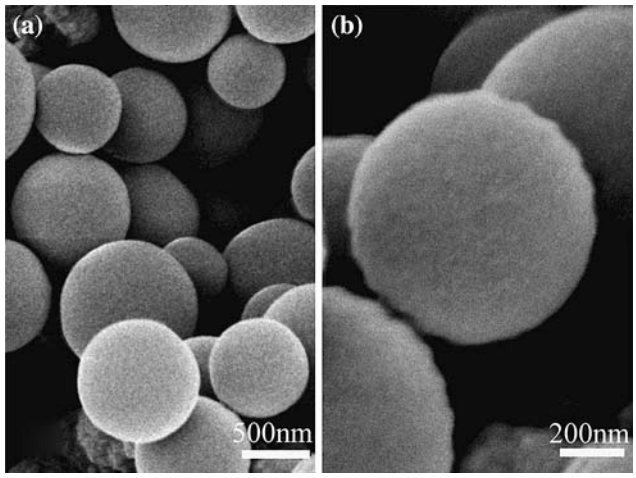

Fig. 2 Annealed at 150 °C

obtained on the substrate instead of bunchy nanoparticles. We can imagine that the bunchy nanoparticles can interlink into microspheres when the quantity of nanoparticles is big enough in the solution. When vaporizing the solution, the bubbles of ammonia gases which decomposed from copper ammine hydroxide can act as moulding board, and thus the bunchy nanoparticles interlink around surface of the bubble and form hollow microspheres. Figures 3 and 4 show the images of the samples annealed at 350 and 500 °C respectively. In Fig. 2, the surface of the microspheres that have been subjected to a low temperature annealing became much smooth. When the annealing temperature reaches to 350 °C and the microspheres become mesoporous with many nanoscaled holes while the size of the microspheres contracts. This leads to the formation of microsphere cages as shown in Fig. 3. The size of both nanoparticles and holes in the microspheres is about 10 nm. Figure 4 shows the image of the sample after annealing at 500 °C. The microsphere cage further contracts slightly while the nanoparticles in the sphere grow up to 40 nm and the holes enlarge accordingly. Many cracked microsphere cages can be observed in Fig. 4, and this may be caused by high temperature annealing.

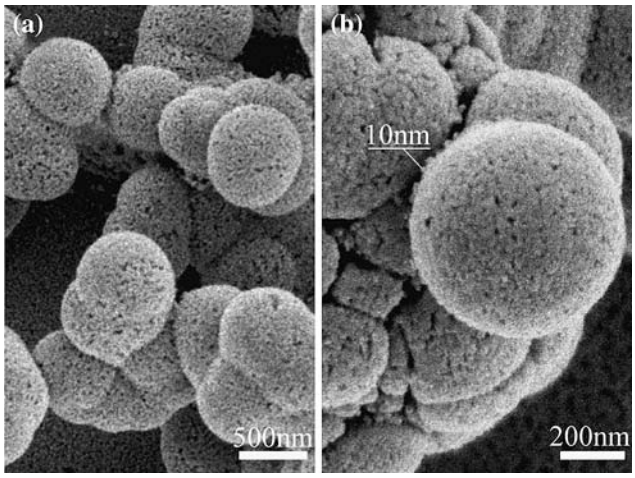

Fig. 3 Annealed at 350 °C

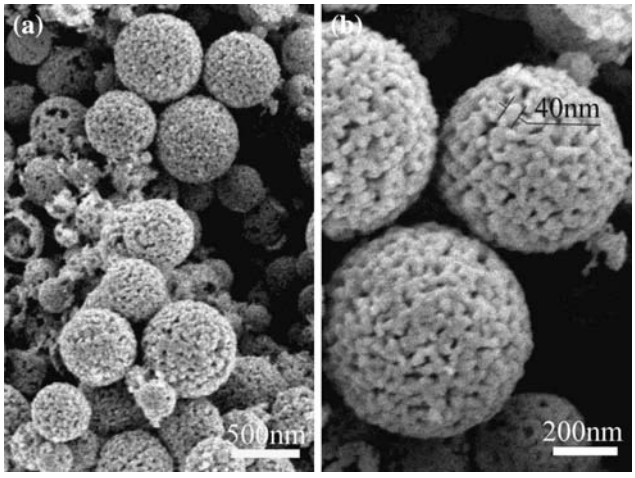

Fig. 4 Annealed at 500 °C

Figure 5 shows the DTA-TG curves of the as-prepared powders from alcohol solution. A distinct weight loss of 25% in the TG curve below 350 °C was measured which corresponded to the decomposition of hydroxide and carbonate. This weight loss starts from room temperature, speeds at 140 °C, reaches it's maximum at 240 °C and corresponds to a large endothermic peak at about 240 °C in the DSC thermograph. There is no weight loss above 350 °C as all the products have been converted to CuO completely.

Figure 6 shows the XRD spectra of the as-prepared samples and these annealed at 150, 350, 500, and 900 °C for 6 h. The sample dried at 80 °C for a long time (5 days) is also shown here. There are three phases indexed in the as-prepared samples, monoclinic tenorite CuO, orthorhombic $Cu(OH)_2$, and monoclinic carbonatodiamminecopper(II) ($Cu(NH_3)_2CO_3$). Because there is 0.03% CO_2 in air, carbonatodiamminecopper(II) can be found in as-prepared samples. After drying for a long time at 80 °C, the peak intensity of both hydroxide and carbonate decreases apparently. When the annealing temperature is above 150 °C, only CuO peaks were observed. Therefore, copper hydroxide and carbonatodiamminecopper(II) decompose and completely convert to CuO. In the DSC-Tg curves of Fig. 5, the decomposing peak is at 240 °C because the rate of temperature rise is as fast as 10 °C/min but the temperature where decomposition occurs is lower than 150 °C. Thus, copper

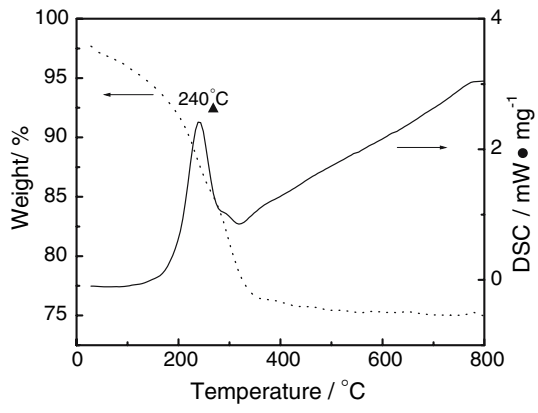

Fig. 5 DTA-TG curves of the as-prepared powders

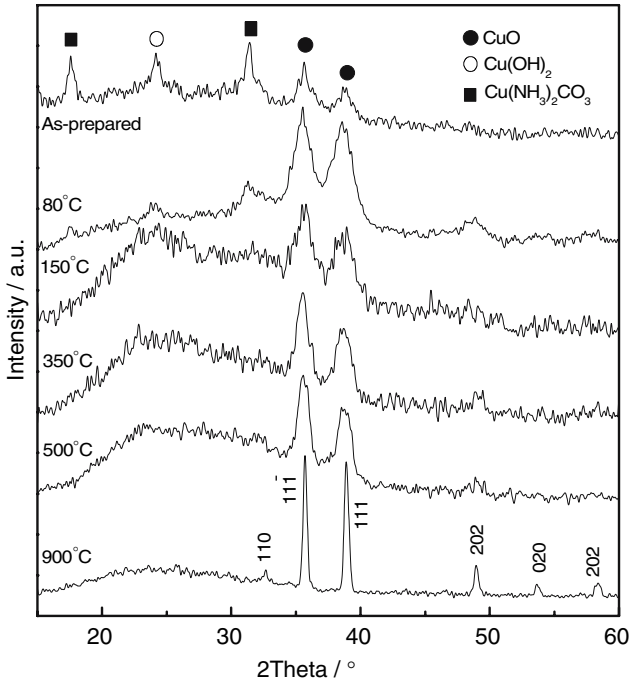

Fig. 6 XRD profile of as-prepared sample and the samples annealing at different temperature.

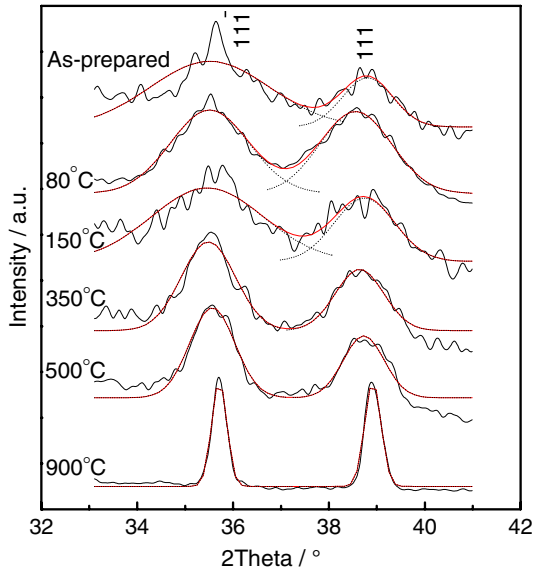

Fig. 7 XRD peaks of ($\bar{1}11$) and (111) of the samples annealed at different temperatures.

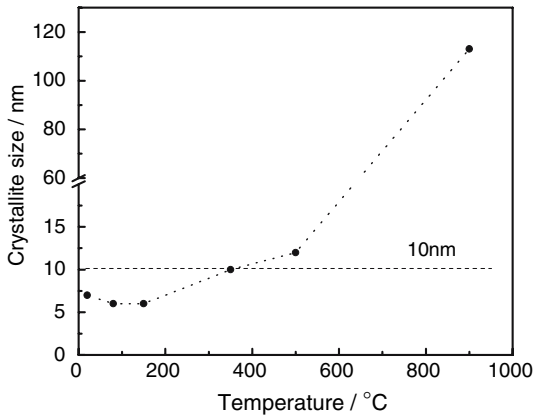

Fig. 8 The annealing temperature dependent of crystallite size

hydroxide and carbonatodiamminecopper(II) can be converted to CuO easily using this method.

The crystallite size of the powders can be estimated from the broadening of corresponding X-ray spectral peaks by the Scherrer's formula

$$L = \frac{K\lambda}{\beta \cos\theta} \tag{2}$$

where L is the crystallite size, λ the wavelength of the X-ray radiation (CuKα = 0.15418 nm), K usually taken as 0.89, β the line width at half-maxiumum height after subtraction of broadening caused by equipment, and θ is the diffraction angle. Here we chose the XRD spectra of ($\bar{1}11$) and (111) plane to estimate their crystallite size and then average them in order to decrease the error of the system. The XRD peaks of monoclinic tenorite CuO ($\bar{1}11$) and (111) of the samples annealed at different temperatures are shown in Fig. 7. The Gaussian fitting was adopted to calculate the half width of XRD peaks.

The annealing temperature dependence of crystallite size is shown in Fig. 8. The crystallite size increases with the annealing temperature. The crystallite size increases slightly at temperature lower than 500 °C, while it increases rapidly at the temperature above 500 °C because of grain growth. This result is in accordance with the FE-SEM observations.

Summary

In summary, we reported a very simple method to convert conventional CuO to nanoparticle interlinked microsphere cages near room temperature by dissolving CuO in aqueous ammonia, followed by vaporizing the solution on a substrate and decomposing ammine compounds. In the sample dip coated once, nanostructures with bunchy nanoparticles of $Cu(OH)_2$ can be formed. After the substrate immerges into the solution and vaporize the solution, hollow microspheres can be formed onto the substrate. There are three phases in the as-prepared samples, monoclinic tenorite CuO, orthorhombic $Cu(OH)_2$, and monoclinic carbonatodiamminecopper(II) ($Cu(NH_3)_2CO_3$). After annealing at

150 °C, all products convert to CuO. When annealed at higher than 350 °C, the microspheres become mesoporous and nanoparticle interlinked microsphere cages can be formed. When the annealing temperatue increase above to 500 °C, some of the microspheres would be cracked and the mesoporous hollowed structures can be clearly observed.

References

1. B. Liu, H.C. Zeng, J. Am. Chem. Soc. **126**(26), 8124 (2004)
2. Z.H. Liang, Y.J. Zhu, Chem. Lett. **34**(2), 214 (2005)
3. Q.Y. Liu, Z.Y. Liu, J. Fan, Chinese. J. Catal. **26**(1), 59 (2005)
4. J. Morales, L. Sanchez, F. Martin, J. Ramos-Barrado, M. Sanchez, Thin. Solid. Films. **474**(1–2), 133 (2005)
5. Y.W. Zhu, T. Yu, F.C. Cheong, X.J. Xui, C.T. Lim, V.B.C. Tan, J.T.L. Thong, C.H. Sow, Nanotechnology **16**(1), 88 (2005)
6. Y. Chang, J.J. Teo, H.C. Zeng, Langmuir **21**(3), 1074 (2005)
7. S. Suarez, J.A. Martin, M. Yates, R. Avila, J. Blanco, J. Catal. **229**(1), 227 (2005)
8. H.W. Hou, Y. Xie, Q. Li, Cryst. Growth Des. **5**(1), 201 (2005)
9. T. Yu, F.C. Cheong, C.H. Sow, Nanotechnology **15**(12), 1732 (2004)
10. S.Z. Li, H. Zhang, Y.J. Ji, D.R. Yang, Nanotechnology **15**(11), 1428 (2004)
11. C.H. Xu, C.H. Woo, S.Q. Shi, Chem. Phys. Lett. **399**(1–3), 62 (2004)
12. S. Bennici, P. Carniti, A. Gervasini, Catal. Lett. **98**(4), 187 (2004)
13. C.H. Lu, L.M. Qi, J.H. Yang, D.Y. Zhang, N.Z. Wu, J.M. Ma, J. Phys. Chem. B **108**(46), 17825 (2004)
14. M.H. Cao, Y.H. Wang, C.X. Guo, Y.J. Qi, C.W. Hu Wang, J. NanoSci. Nanotech. **4**(7), 824 (2004)
15. J.W. Zhu, H.Q. Chen, H.B. Liu, X.J. Yang, L.D. Lu, W. Xin, Mater. Sci. Engr. A **384**(1–2), 172 (2004)
16. Z.H. Liang, Y.J. Zhu, Chem. Lett. **33**(10), 1314 (2004)
17. R. Yang, L. Gao, Chem. Lett. **33**(9), 1194 (2004)
18. G.H. Du, G. Van Tendeloo, Chem. Phys. Lett. **393**(1–3), 64 (2004)
19. A.O. Musa, T. Akomolafe, M.J. Carter, Sol. Energ. Mater. Sol. C **51**, 305 (1998)
20. M. Muhibbullah, M.O. Hakim, M.G.M. Choudhury, Thin Solid Films **423**, 103 (2003)
21. J. Ziolo, F. Borsa, M. Corti, A. Rigamonti, F. Parmigiani, J. Appl. Phys. **67**, 5864 (1990)
22. T.J. Huang, T.C. Yu, Appl. Catal. **71**, 275 (1991)
23. H. Hamada, Y. Kintaichi, M. Sasaki, T. Ito, M. Tabata, Appl. Catal. **75**, L1 (1991)
24. H. He, P. Bourges, Y. Sidis, C. Ulrich, L.P. Regnault, S. Pailhes, N.S. Berzigiarova, N.N. Kolesnikov, B. Keimer, Science **295**, 1045 (2002)
25. K.M. Lang, V. Madhavan, J.E. Hoffman, E.W. Hudson, H. Eisaki, S. Uchida, C. Davis, Nature **415**, 412 (2002)
26. P. Novak, Electrochim. Acta. **31**, 1167 (1986)
27. J.R. Ortiz, T. Ogura, J. Medina-Valtierra, S.E. Acosta-Ortiz, P. Bosh, J.A. de las Reyes, V.H. Lara, Appl. Surf. Sci. **174**, 177 (2001)
28. K.C.C. Kharas, Appl. Catal. B Environ. **2**, 207 (1993)
29. R.B. Vasiliev, M.N. Rumyantseva, N.V. Yakovlev, A.M. Gaskov, Sens. Actua. B Chem. **50**, 186 (1998)
30. Y. Nakamura, H. Zhuang, A. Kishimoto, O. Okada, H. Yanagida, J Electrochem. Soc. **145**, 632 (1998)
31. D.W. Kim, B. Park, J.H. Chung, K.S. Hong, Jpn. J. Appl. Phys. **39**, 2696 (2000)
32. Pan Zhengwei, Dai Zurong, Wang Zhonglin, Science **291**, 1947 (2000)
33. Y. Zhou, S.H. Yu, X.P. Cui, C.Y. Wang, Z.Y. Chen, Chem. Mater. **11**, 545 (1999)
34. J.J. Zhu, S.W. Liu, O. Palchik, Y. Koltypin, A. Gedanken, Langmuir **16**, 6396 (2000)
35. G.H. Du, Q. Chen, P.D. Han, L.M. Peng, Phys. Rew. B **67**, 035323 (2003)
36. G.H. Du, L.M. Peng, Q. Chen, S. Zhang, W.Z. Zhou, Appl. Phys. Lett. **83**, 1638 (2003)
37. J.Q. Qi, T. Zhang, M. Lu, Y. Wang, W.P. Chen, L.T. Li, H.L.W. Chan, Chem. Lett. **34**(2), 180 (2005)